Published July 11, 2011

Spatial organization of RYRs and BK channels underlying the activation of STOCs by Ca^{2+} sparks in airway myocytes

Lawrence M. Lifshitz,[1,3] Jeffrey D. Carmichael,[1,3] F. Anthony Lai,[4] Vincenzo Sorrentino,[5] Karl Bellvé,[1,3] Kevin E. Fogarty,[1,3] and Ronghua ZhuGe[1,2]

[1]Biomedical Imaging Group, [2]Department of Microbiology and Physiological Systems, and [3]Program in Molecular Medicine, University of Massachusetts Medical School, Worcester, MA 01605
[4]Wales Heart Research Institute, Cardiff University School of Medicine, Cardiff CF14 4XN, Wales, UK
[5]Department of Neuroscience, University of Siena, Siena 53100, Italy

Short-lived, localized Ca^{2+} events mediate Ca^{2+} signaling with high efficiency and great fidelity largely as a result of the close proximity between Ca^{2+}-permeable ion channels and their molecular targets. However, in most cases, direct evidence of the spatial relationship between these two types of molecules is lacking, and, thus, mechanistic understanding of local Ca^{2+} signaling is incomplete. In this study, we use an integrated approach to tackling this issue on a prototypical local Ca^{2+} signaling system composed of Ca^{2+} sparks resulting from the opening of ryanodine receptors (RYRs) and spontaneous transient outward currents (STOCs) caused by the opening of Ca^{2+}-activated K^+ (BK) channels in airway smooth muscle. Biophysical analyses of STOCs and Ca^{2+} sparks acquired at 333 Hz demonstrate that these two events are associated closely in time, and approximately eight RYRs open to give rise to a Ca^{2+} spark, which activates ∼15 BK channels to generate a STOC at 0 mV. Dual immunocytochemistry and 3-D deconvolution at high spatial resolution reveal that both RYRs and BK channels form clusters and RYR1 and RYR2 (but not RYR3) localize near the membrane. Using the spatial relationship between RYRs and BK channels, the spatial-temporal profile of $[Ca^{2+}]$ resulting from Ca^{2+} sparks, and the kinetic model of BK channels, we estimate that an average Ca^{2+} spark caused by the opening of a cluster of RYR1 or RYR2 acts on BK channels from two to three clusters that are randomly distributed within an ∼600-nm radius of RYRs. With this spatial organization of RYRs and BK channels, we are able to model BK channel currents with the same salient features as those observed in STOCs across a range of physiological membrane potentials. Thus, this study provides a mechanistic understanding of the activation of STOCs by Ca^{2+} sparks using explicit knowledge of the spatial relationship between RYRs (the Ca^{2+} source) and BK channels (the Ca^{2+} target).

INTRODUCTION

Intracellular Ca^{2+} concentration ($[Ca^{2+}]_i$) serves as a versatile signal to mediate a remarkable array of cellular processes, including neurotransmitter and hormone secretion, muscle contraction, and gene regulation. To fulfill such diverse functions, cells evolve many strategies to generate Ca^{2+} signals tailored to specific cellular functions (Berridge et al., 2003). One such strategy is to organize Ca^{2+}-permeable channels and their targets in proximity, forming so-called Ca^{2+} nano- and microdomains, such that Ca^{2+} only activates the targets within the domain. Because of the closeness between the Ca^{2+} source and its targets, many processes governing global Ca^{2+} signaling become ineffective in local Ca^{2+} signaling (Neher, 1998). For example, because Ca^{2+} diffusion from Ca^{2+} sources often results in steep gradients in $[Ca^{2+}]$, the distance between Ca^{2+} sources and targets exerts a critical influence on the efficacy and fidelity of signal transduction, as does the sensitivity of the targets to Ca^{2+}. Although the Ca^{2+} profile created by local Ca^{2+} events is understood to a great extent, the spatial relationships between Ca^{2+} sources and their targets are not determined experimentally in most cases, and the understanding of localized Ca^{2+} signaling is thus incomplete.

A prototypical example of local Ca^{2+} signaling is Ca^{2+} sparks and spontaneous transient outward current (STOC) in smooth muscle and neurons (Brown et al., 1983; Nelson et al., 1995; Bolton and Imaizumi, 1996). Ca^{2+} sparks are highly localized, short-lived Ca^{2+} transients because of the opening of RYRs on the membrane of endo/sarcoplasmic reticulum. In smooth muscle cells, Ca^{2+} sparks activate large-conductance Ca^{2+}-activated K^+ (BK) channels to give rise to STOCs. Depending on the type of smooth muscle, spark-STOC signaling renders a different physiological function. In vascular smooth muscle from the cerebral artery, functional coupling of sparks to STOCs hyperpolarizes the membrane

Correspondence to Ronghua ZhuGe: Ronghua.zhuge@umassmed.edu

Abbreviations used in this paper: ASM, airway smooth muscle; STIC, spontaneous transient inward current; STOC, spontaneous transient outward current; VDCC, voltage-dependent Ca channel.

The Rockefeller University Press $30.00
J. Gen. Physiol. Vol. 138 No. 2 195–209
www.jgp.org/cgi/doi/10.1085/jgp.201110626

Supplemental Material can be found at:
http://jgp.rupress.org/content/suppl/2011/07/10/jgp.201110626.DC1.html

Published July 11, 2011

potential, which in turn shuts off voltage-dependent Ca channels (VDCCs), leading to the decrease in global [Ca^{2+}] and relaxation (Nelson et al., 1995). In ureteral smooth muscle, the activation of STOCs by Ca^{2+} sparks limits the availability of VDCCs, resulting in a prolonged action potential refractory period (Burdyga and Wray, 2005). Finally, because of their capability to also turn on spontaneous transient inward currents (STICs), which counteracts the STOC, Ca^{2+} sparks serve as a membrane potential stabilizer in smooth muscle from airway, portal vein, and corpora cavernosa (Hogg et al., 1993; Van Helden, 1993; Janssen and Sims, 1994; ZhuGe et al., 1998; Karkanis et al., 2003; Bao et al., 2008). The critical role of Ca^{2+} sparks and STOCs in smooth muscle contractility is heightened by the findings that uncoupling or suppressing the coupling between them leads to hypertension, urinary incontinence, and retinopathy (Brenner et al., 2000; Plüger et al., 2000; Amberg et al., 2003; Meredith et al., 2004; McGahon et al., 2007).

In spite of the physiological importance and pathological implications of Ca^{2+} sparks and STOCs in smooth muscle, the spatial organization of BK channels and RYRs is still poorly understood. However, this knowledge is critical to understanding how Ca^{2+} sparks activate STOCs. Previously, we estimated that in amphibian gastric smooth muscle, BK channels are exposed to 10 µM [Ca^{2+}] during a Ca^{2+} spark, leading to a suggestion that RYRs and BK channels form a microdomain in which BK channels are at a higher density than other regions of the cells (ZhuGe et al., 1999, 2002). Interestingly, although Pérez et al. (2001) derived that BK channels in cerebral smooth muscle cells are activated by a similar level of [Ca^{2+}] caused by Ca^{2+} sparks, these authors proposed that BK channels localize homogeneously in the surface membrane and that a Ca^{2+} spark activates them localized in an area of 13 μm^2. This leads to a possibility that there might be a difference between amphibian and mammalian cells with regards to the distribution of BK channels in the Ca^{2+} spark domains. Such a difference should also motivate an analysis that can directly localize and visualize RYRs and BK channels in smooth muscle cells.

In the present study, we have investigated the spatial relationship between RYRs and BK channels that underlies the functional coupling between Ca^{2+} sparks and STOCs in airway smooth muscle (ASM) cells from mice. To address this question more precisely, we used two complementary approaches: (1) dual immunocytochemistry to visualize the distribution of BKs and RYRs and (2) functional analysis of the quantitative relationship between sparks and STOCs. For the immunocytochemistry, we used isoform-specific RYR antibodies to determine the 3-D cellular distribution of these proteins at high spatial resolution. For the functional analysis, we simultaneously imaged Ca^{2+} sparks at 333 Hz and recorded corresponding STOCs at 1 KHz so a detailed analysis of their relationship could be performed. With the combination of these approaches, we found that (a) RYR1 and RYR2 localize near the plasma membrane while RYR3 localizes near the nucleus, so only RYR1 and RYR2 appear functionally able to couple with BK channels; (b) both RYRs and BK channels form clusters; and (c) for a given RYR1 or RYR2 cluster, two to three BK clusters on average are randomly distributed within the region where the [Ca^{2+}] is high enough to produce STOC-like events. Combining a kinetic model of BK channels, the spatial-temporal Ca^{2+} profile generated by sparks, and the spatial organization of RYRs and BK channels, we can recapitulate the essential features of STOCs activated by Ca^{2+} sparks. Therefore, we are able to provide a mechanistic explanation of Ca^{2+} spark–induced STOC based on the physical relationship of these channels in the same type of cells.

MATERIALS AND METHODS

Preparation of ASM cells from mice

Male Swiss Webster mice from 6 to 10 wk of age were anaesthetized with 50 mg kg^{-1} intrapertoneally injected pentobarbitone. After each animal was unresponsive to any applied stimulus, the trachea was quickly removed and placed in a prechilled dissociation solution consisting of 135 mM NaCl, 6 mM KCl, 5 mM $MgCl_2$, 0.1 mM $CaCl_2$, 0.2 mM EDTA, 10 mM HEPES, and 10 mM glucose, pH 7.3. This method is in accordance with the guidelines of the Animal Care Committee of the University of Massachusetts Medical School and is consistent with the recommendation of the Panel on Euthanasia of the American Veterinary Medical Association. The tracheas were dissected free from the surface of the connective tissue. The tissue was then incubated in the dissociation medium containing 30 U/ml papain (Sigma-Aldrich), 1 mM dithiothreitol, and 0.5 mg/ml BSA at 35°C for 30 min. The tissue was then transferred to a dissociation medium containing 3 U/ml collagenase F (Sigma-Aldrich) and 0.5 mg/ml BSA and incubated at 35°C for another 15 min to produce isolated ASM cells. Finally, the tissue was agitated with a fire-polished wide-bore glass pipette to release the cells. The isolated single ASM cells were used on the same day at room temperature (22–25°C).

Patch-clamp recording

Membrane currents were recorded using the tight-seal, whole-cell patch recording configuration. The extracellular solution contained 130 mM NaCl, 5.5 mM KCl, 2.2 mM $CaCl_2$, 1 mM $MgCl_2$, and 10 mM HEPES, pH adjusted to 7.4 with NaOH. The pipette solution contained 139 mM KCl, 1 mM $MgCl_2$, 10 mM HEPES, 3 mM Na_2ATP, and 0.05 mM fluo-3, pH adjusted to 7.3 with KOH. For experiments in Fig. 8, 40 mM NaCl was replaced by 40 mM KCl to set E_k at −28 mV, and niflumic acid at 50 µM was added to block the STICs (Hogg et al., 1994; Janssen and Sims, 1994). Whole-cell currents were recorded at a holding potential of 0 mV, low-pass filtered using the Axopatch 1D amplifier (Molecular Devices; 200-Hz cutoff), and then digitally sampled at 1 kHz and stored for analysis. Events were counted as STOCs if they exceeded a threshold of 10 pA as detected by Mini analysis software (Synaptosoft, Inc.). The events were then visually inspected to eliminate anomalies such as multiple events overlapping in time or excessively noisy traces.

Imaging and measurement of Ca^{2+} sparks

Fluorescent images were obtained using fluo-3 as the Ca indicator and a custom-built wide-field, high speed digital imaging system (ZhuGe et al., 1999). Rapid imaging was made possible by using a

Published July 11, 2011

cooled high sensitivity charge-coupled device camera (128 × 128 pixels) developed in conjunction with the Massachusetts Institute of Technology Lincoln Laboratory. The camera was interfaced to a custom-made inverted microscope equipped with a 60× oil immersion lens (numerical aperture of 1.3), with each pixel covering a 333 × 333–nm area of the cell. The 488-nm line of a multiline argon laser provided fluorescence excitation for the indicator fluo-3, and a laser shutter controlled the exposure duration. Emission of the Ca^{2+} indicator was monitored at wavelengths >500 nm. To obtain a constant concentration of Ca^{2+} indicator, 50 µM fluo-3 was delivered through the patch pipette, and measurements were not commenced until 10–15 min after disruption of the patch. After this time, no significant change in background fluorescence was detected. Subsequent image processing and analysis were performed off line using a custom-designed software package running on a PC.

Two measures of Ca^{2+} sparks were used: (1) the conventional fluorescence ratio, $\Delta F/F_0$, within a restricted volume, and (2) the change in total fluorescence, $F - F_o$, over a larger volume (i.e., 40 × 40 pixels, 333 nm/pixel), also designated as the Ca^{2+} signal mass, which is proportional to the total quantity of Ca^{2+} released into the cytosol. These measurements have been previously described (ZhuGe et al., 2000, 2002). The endogenous fixed Ca^{2+} buffer as estimated in Bao et al. (2008) was taken into account to calculate $[Ca^{2+}]$.

Simulation of the spatial-temporal profile of $[Ca^{2+}]$ arising from Ca^{2+} sparks

To gain insight into the possible role of Ca^{2+} sparks, we modeled a cell and simulated sparks and examined the spatial and temporal profile of free Ca^{2+} that resulted at the plasma membrane where BK channels would localize. Finite difference approximations were used to solve a set of partial differential equations for the reaction-diffusion kinetics in a cylindrical coordinate system. The details of this approach were described previously (ZhuGe et al., 2000, 2002). The cell was modeled as a cylinder, 6 µm in diameter and 3 µm in height. The Ca^{2+} release site was modeled as a small cylinder, 20 nm in radius and height, with its end 20 nm from the plasma membrane. Three $I_{Ca(spark)}$s with the same waveform (a linear rise time of 9 ms and an exponential decay with a τ of 12 ms) and different amplitudes (i.e., 1.12, 3.36, and 10.08 pA) were used as input Ca^{2+} currents. This waveform and these amplitudes for $I_{Ca(spark)}$ were selected to match and reflect measured $I_{Ca(spark)}$s in this study and in Bao et al. (2008). The total concentration of fixed and slowly diffusible buffers and the on and off kinetics were taken to be those determined by us in the same cells (Bao et al., 2008).

Reverse transcription PCR detection of mRNA for three types of RYRs

The trachea from mice was carefully isolated, quickly removed of connective tissue and epithelium, and then frozen in dry ice. The total RNA of the trachea was isolated with the TRIZOL (Invitrogen) method according to the manufacturer's guidelines, and cDNA was synthesized using extracted RNA with an Omniscript Reverse Transcription kit (QIAGEN). The specific primers for mouse RYR1, RYR2, RYR3, and for β-actin have been described previously (ZhuGe et al., 2006) and were synthesized by Invitrogen. β-Actin was used as a positive control and the absence of DNA as a negative control, and the PCR reaction was performed in a PCR mastercycler (model 5332; Eppendorf). The PCR was held at 94°C for 30 s and then cycled 35 times, with each cycle consisting of 93°C for 30 s, 54°C for 30 s, and 72°C for 30 s. The hippocampus for the same animal was dissected and checked for RYR mRNA with the same protocol as in ASM.

3-D visualization of RYRs and BK channels

Immunocytochemistry was performed as described previously (ZhuGe et al., 2006). Polyclonal rabbit antibodies for RYRs were generated using the epitopes RREGPRGPHLVGPSRC for RYR1 (Mitchell et al., 2003) and KAALDFSDAREKKKPKKDSSLSAV for RYR2 (Tunwell et al., 1996). The polyclonal rabbit anti-RYR3 antibody was developed against purified glutathione-*S*-transferase fusion protein corresponding to the region of low homology between the transmembrane domains 4 and 5 of RYR3 (Giannini et al., 1995). Preimmune serum was used as negative controls of anti-RYRs. BK channel antibody was purchased from BD. The immunogen for this anti-BK channel is residues 995–1,113 of human $BK_{Ca}\alpha$, and the specificity of this antibody has been confirmed in the studies of several cell types and tissues (i.e., Samaranayake et al., 2004; Lim and Park, 2005; Brainard et al., 2005). Mouse preimmune IgG was used as a negative control for the anti-BK channel.

3-D fluorescence imaging was performed on an inverted widefield microscope (Diaphot 200; Nikon) with excitation by a 100-W mercury lamp. Images were obtained through a 60× objective and digitally recorded on a cooled, back-thinned charge-coupled device camera (CH250; Photometrics) with an effective pixel size at the specimen of 80 nm in x-y and a z spacing of 250 nm. This resulted in a 3-D stack of ~40 image planes for each cell.

The fluorescence images were deconvolved with a constrained, iterative approach originally designed for UNIX systems (Carrington et al., 1995). The algorithm was rewritten using FFTW, a free, fast-Fourier transform library, and implemented as a multiuser client/server system on computers running the Fedora operating system (Red Hat), either stand alone or configured in a Beowulf cluster. Each image was dark current and background subtracted, flat-field corrected, and then deconvolved. After deconvolution, images were thresholded to eliminate nonspecific binding. Voxels that fell below a threshold were considered to be nonspecific bindings and were set to zero; all other voxels remained unchanged. This threshold was derived from analysis of control images containing no primary antibody and only secondary label. The intensity that eliminates 99% of voxels in the control images became the threshold intensity.

As shown in the Results, positive immunostained objects for RYRs and BK channels consist of multiple voxels. We call this group of voxels a punctum. Our functional analyses revealed that each punctum is made of multiple channels, and we call all of the channels in a punctum a cluster.

Because an image voxel has (x, y, and z) dimensions of 80 × 80 × 250 nm, we considered two possibilities in our calculation of the area that a punctum might encompass on the plasma membrane (its plasma membrane area). For one, we assumed all punctum voxels present their xy face to the plasma membrane. In this case, the plasma membrane area of each voxel was 80 × 80 nm. For the other, we assumed that the xz or yz face was on the plasma membrane, producing a plasma membrane area of 80 × 250 nm.

Simulation of BK channel currents in response to Ca^{2+} sparks

Simulations of BK channel activation were performed by integrating a set of partial differential equations. The differential equations were written in the xppaut syntax and solved using the free xppaut software (Ermentrout, 2002). The steady-state open probability ($P_{o,ss}$) for a BK channel was taken to be that described by Bao and Cox (eq. 14 in Bao and Cox, 2005). This is a function of $[Ca^{2+}]$ and voltage. At each instant in time, the P_o is driven toward this steady-state value at a simple exponential rate (based on an experimentally observed time constant of τ) as Marhl et al. (2006) did but using a different P_o. This τ itself is a function of local $[Ca^{2+}]$ and thus is usually changing. Mathematically, $dP_o/dt = (P_{o,ss} - P_o)/\tau$, where τ is $\tau(Ca)$ and $P_{o,ss}$ is $P_{o,ss}(Ca, V)$. As $[Ca^{2+}]$ changes as a result of release from the spark, τ and $P_{o,ss}$ will change. If $P_o(t) < P_{o,ss}$, an activation τ based on the opening rate of BK channels is used; otherwise, a deactivation τ based on the closing rate is used (see Figs. 7 and 8). The simulation does not contain any explicit spatial component; distance from a spark to a BK cluster is incorporated by the choice of $[Ca(t)]$ to which each cluster is exposed.

Published July 11, 2011

To simulate the STOC initiated by Ca^{2+} release from one RYR cluster, we first determined the distance to all nearby BK channel clusters. This is necessary because each BK cluster is at a different distance from RYRs, and therefore each is exposed to a different Ca(t) profile. Each BK cluster in the simulation possesses its own P_o that is driven by its appropriate Ca(t) profile (based on its distance from the RYR). As the simulation runs, the current though each BK channel cluster is calculated as $I_{BK} = N \times \gamma \times P_o \times V$, where N is the number of BK channels in a cluster (assumed to be 10; see Results), γ is single-channel conductance, V is the driving voltage, and P_o is the P_o for that specific BK cluster. The currents through all nearby BK channel clusters are then added to generate STOCs.

Data analyses

Results are reported as means ± SEM unless noted otherwise. Statistic analyses were performed using Origin version 7.5. Linear regression used a weighted least-square method to fit a linear model function of data. When appropriate, one-way ANOVA followed by *t* tests was used to compare means. The significance level was set at the 0.05 level.

Online supplemental material

Fig. S1 tests BK channel kinetics at different voltages in response to $[Ca^{2+}]$ jumps between 1 and 320 µM. Fig. S2 compares the effects of $I_{Ca(spark)}$ amplitude on simulated and measured STOCs. Fig. S3 examines the voltage dependence of $P_o(t)$ of BK channels from the puncta marked in Fig. 5 A. Video 1 shows the 3-D distribution of RYR3 and BK channels. Video 2 shows the 3-D distribution of RYR1. Video 3 shows the 3-D distribution of RYR2. Video 4 shows the spatial relationship between RYR2s and BK channels. Video 5 displays the evolution of a Ca^{2+} spark acquired at 333 Hz. Online supplemental material is available at http://www.jgp.org/cgi/content/full/jgp.201110626/DC1.

RESULTS

The overall goals of this study were to (a) quantify the functional relationship between Ca^{2+} sparks and STOCs, (b) visualize and determine the spatial relationship between RYRs and BK channels, and (c) integrate the results from a and b with BK channel kinetics and the $[Ca^{2+}]$ profile generated by Ca^{2+} sparks to establish a model that recapitulates features of STOCs.

Temporal closeness between Ca^{2+} sparks and STOCs

In ASM, Ca^{2+} sparks activate BK channels to generate STOCs and Ca^{2+}-activated Cl^- channels to give rise to STICs (ZhuGe et al., 2010). To obtain insight into the relationship between Ca^{2+} sparks and STOCs, two approaches were used. First, the cells were voltage clamped at the reversal potential for Cl^- (E_{Cl}, 0 mV) so STICs would not occur. Second, Ca^{2+} sparks were recorded at 333 Hz so their temporal relationship with STOCs could

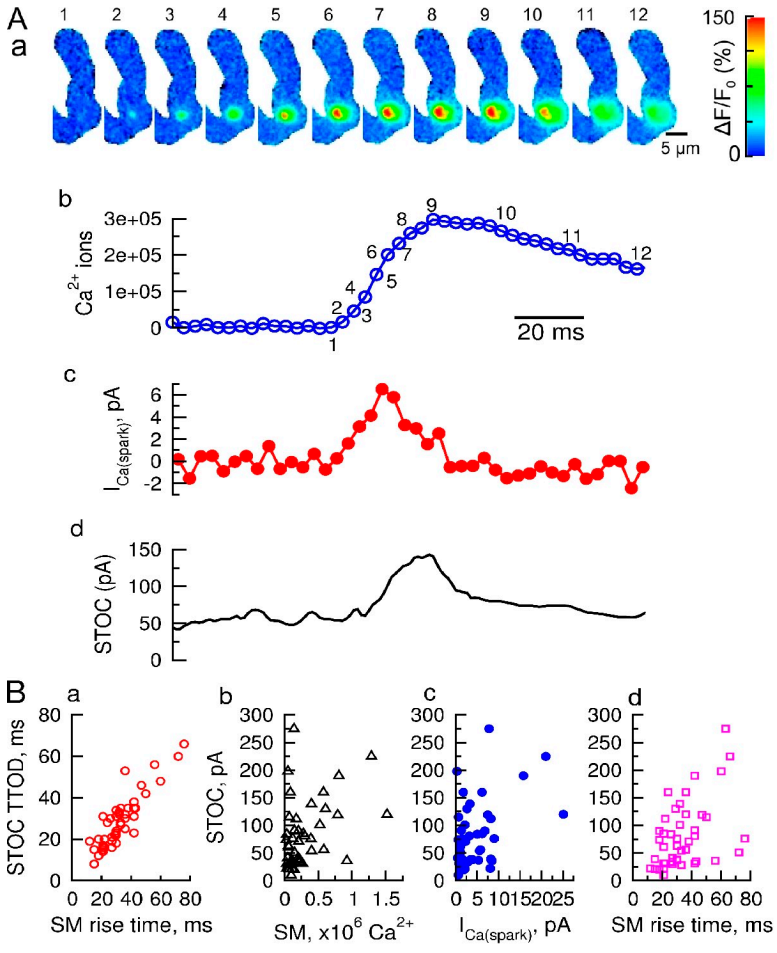

Figure 1. Relationship between Ca^{2+} sparks and their corresponding STOCs. The cells were voltage clamped at 0 mV, and the images were acquired at 333 Hz with an exposure time of 3 ms. Cytosolic Ca^{2+} was measured using 50 µM fluo-3, which was introduced into the cells in the K^+ form through the patch pipette. (A) Temporal relationship between a STOC and a Ca^{2+} spark. Images (a) display the spatio-temporal evolution of the Ca^{2+} spark (Video 5). Changes in $[Ca^{2+}]$ in the images are expressed as $\Delta F/F_0$ (percentage) and displayed on a pseudocolor scale calibrated at the right. The traces shown are the time course of signal mass (b), its time derivative calibrated to give the underlying Ca^{2+} current flowing from the intracellular Ca^{2+} store into the cytosol, i.e., $I_{Ca(spark)}$ (c), and the corresponding STOC (d). The numbers above the images correspond to the time when images were acquired as indicated in the time course of signal mass. Note that the endogenous Ca^{2+} buffer as estimated in Bao et al. (2008) was taken into account in this and in Fig. 2's calculation of signal mass and $I_{Ca(spark)}$. (B) Quantitative relationships between Ca^{2+} sparks and STOCs. Scatter plots show the correlations between (a) the rise time of Ca^{2+} spark signal mass (SM) and the time between the onset of the STOC and the onset of its decay, designated as time to the onset of decay (TTOD; r = 0.8869, P < 0.0001); (b) signal mass and STOC amplitude (r = 0.404, P = 0.005), (c) $I_{Ca(spark)}$ and STOC amplitude (r = 0.4451, P = 0.002), and (d) signal mass rise time and STOC amplitude (r = 0.4816, P = 0.001). *n* = 35 in all panels.

Published July 11, 2011

be determined with more accuracy. With these approaches, we detected a close temporal correlation between Ca^{2+} sparks and STOCs (Fig. 1 A). The onset of Ca^{2+} sparks coincided with the onset of a STOC or preceded it by 3 ms on average (range of 0–12 ms, $n = 35$). The rise time of Ca^{2+} spark signal mass was 32 ± 2 ms, which was not significantly different from $TTOD_{STOC}$ (time from the onset of the rise to the onset of the decay of STOCs; 29 ± 2 ms; P = 0.148, $n = 35$; Fig. 1 B, a). Such close temporal correlation suggests that RYRs underlying Ca^{2+} sparks and BK channels underlying STOCs localize in proximity to each other in these cells.

Relationship between the amplitude of Ca^{2+} sparks and STOCs

By combining the derivative of the signal mass with knowledge of the cell's Ca buffering capacity, reaction-diffusion simulations, and fluo-3 fluorescence intensity, we can derive $I_{Ca(spark)}$ (ZhuGe et al., 2000). On average, $I_{Ca(spark)}$ has an amplitude of 2.8 ± 0.4 pA with a linear rise peaking at 11 ± 1.1 ms and a single exponential decay with a τ of 12 ± 1.4 ms ($n = 13$) when cells were held at 0 mV. With signal mass and $I_{Ca(spark)}$, we further analyzed the relationship between Ca^{2+} sparks and STOCs. As shown in Fig. 1, there exist weak, yet significant, correlations between Ca^{2+} spark signal mass and STOC amplitude (r = 0.404, P = 0.005; Fig. 1 B, b), between peak $I_{Ca(spark)}$ and STOC amplitude (r = 0.4451, P = 0.002; Fig. 1 B, c), and between rise time of signal mass and STOC amplitude (r = 0.4816, P = 0.001; Fig. 1 B, d). The weakness of the correlations implies that either BK channels are so close to RYRs that they are saturated by Ca^{2+} or that the coupling between BK channels and RYRs varies significantly in number and/or in spatial proximity. Other evidence supports the latter of these two possibilities (see below).

Decay of STOCs is determined by the kinetics of BK channels

Our previous study in amphibian gastric stomach cells indicated that BK channel kinetics plays a key role in determining the decay of STOCs (ZhuGe et al., 2002) because $[Ca^{2+}]$ is very low during the STOC decay. If this is also the case in ASM, we would expect that (a) the

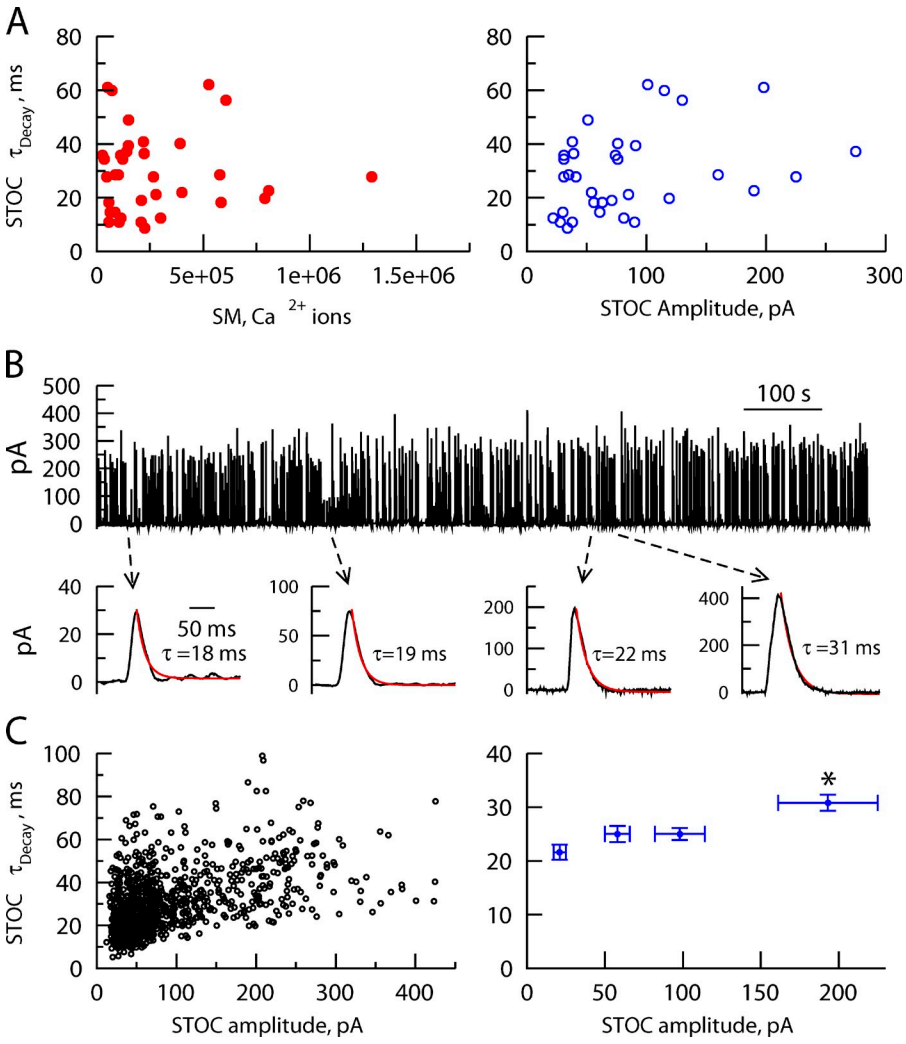

Figure 2. STOC decay reflects the kinetics of BK channels. (A) No correlation between signal mass (SM) and STOC decay (left; r = 0.0091, P = 0.9588, $n = 35$) and between STOC amplitude and STOC decay (right; r = 0.3227, P = 0.0587, $n = 35$). The parameters were calculated from the data shown in Fig. 1. (B) A long recording of STOCs at 0 mV. Arrows depict the time when the events in the inserts occurred. Note that STOCs with different amplitudes can be fitted with a single exponential (solid red lines) with similar time constants. (C) Scatter plot of STOC amplitude and decay for the events from B (left). Mean data reveal that, except for the STOCs in the largest quartile, STOC decay is independent of its amplitude (right). *, P < 0.05 compared with other groups, *t* test after ANOVA; $n = 8$ cells.

Published July 11, 2011

decay of STOCs would follow a single exponential function with a time constant close to the mean open time of BK channels and (b) the decay of STOCs would be independent of their own amplitude and Ca^{2+} spark amplitude. We tested these possibilities by first examining STOCs and their corresponding Ca^{2+} sparks. STOC decay can be fitted with a single exponential with a τ of 29 ± 3 ms (n = 45), which is close to the mean open time of BK channels in smooth muscle (Singer and Walsh, 1987; Tanaka et al., 1997; Harper et al., 2001; Lu et al., 2008; Yang et al., 2009). Moreover, no correlation between signal mass and STOC decay was present (r = 0.0091, P = 0.9588, n = 35; Fig. 2 A), nor was STOC amplitude and STOC decay correlated (r = 0.3227, P = 0.0587, n = 35; Fig. 2 A).

To confirm these results with a much larger sample size, we recorded STOCs without imaging Ca^{2+} sparks. In the cell shown in Fig. 2 B, 991 events from an ∼30-min recording were detected and analyzed. Strikingly, STOCs varied by a factor of 10 in amplitude but decayed with time constants that differ by less than a factor of 2 (Fig. 2, B and C), suggesting that the decay of STOCs is not dependent on the amplitude of STOCs. Given the large variation in the STOC amplitude, we ranked STOCs by their amplitude and grouped them by quartile. On average, τ values for STOC decay were 22 ± 1.4, 23 ± 1.5, 25 ± 1.1, and 31 ± 1.5 ms (n = 8 cells) from the smallest quartile to the largest (Fig. 2 C). Among the first three quartiles in which mean STOC amplitudes varied by threefold, no statistically significant difference in decay rate was detected. Although the decay in the largest quartile was somewhat longer than the first three groups, it still fell within the range of the mean open time of BK channels reported in smooth muscle (Singer and Walsh, 1987; Tanaka et al., 1997; Harper et al., 2001; Lu et al., 2008; Yang et al., 2009). The results in Fig. 2 indicate that STOC decay reflects the closing rate constant of BK channels and thus is determined by the BK kinetics and not by residual [Ca^{2+}] upon termination of Ca^{2+} sparks. This conclusion is supported by the STOC simulations based on the spatial relationship between RYRs and BK channels (see Fig. 7).

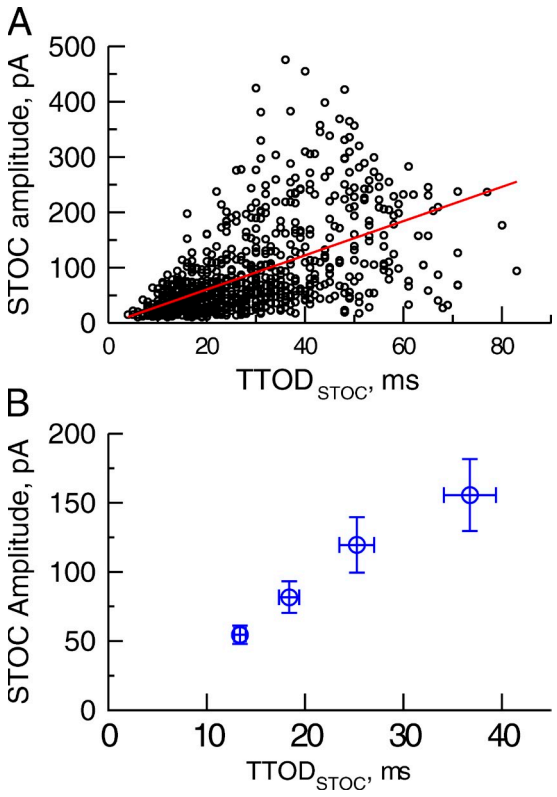

Figure 3. STOC amplitude is correlated with $TTOD_{STOC}$. STOCs are from the data shown in Fig. 2 C. (A) The relationship between $TTOD_{STOC}$ and STOC amplitude (r = 0.5720, P < 0.0001, n = 954 events). (B) Quartile analysis of $TTOD_{STOC}$ and STOC amplitude (n = 8 cells).

Relationship between $TTOD_{STOC}$ and STOC amplitude

Using reaction-diffusion modeling, we have previously shown that the rise time of signal mass equals the duration of $I_{Ca(spark)}$ (ZhuGe et al., 2000). As shown in Fig. 1 B, the rise time of signal mass is the same as $TTOD_{STOC}$ (Fig. 1 B); we reason that $TTOD_{STOC}$ should reflect the duration of $I_{Ca(spark)}$. Therefore, by examining the relationship between $TTOD_{STOC}$ and STOC amplitude, we can infer the relationship between the duration of $I_{Ca(spark)}$ and the magnitude of STOCs. Fig. 3 B demonstrates that there was a positive correlation between $TTOD_{STOC}$ and STOC amplitude for the events shown in Fig. 2 A (r = 0.5561, P = 0.0001). This correlation is also evident in the averaged data in which STOCs were divided into quartiles based on their rank order of $TTOD_{STOC}$; i.e., the longer the $TTOD_{STOC}$, the greater the STOC amplitude (ANOVA, P < 0.05). Therefore, the duration of $I_{Ca(spark)}$ contributes to the amplitude of STOCs. This relationship implies that (a) activation kinetics plays a role in determining the amplitude of STOCs and (b) additional recruitment of BK channels is possible by longer duration of Ca^{2+} sparks. To corroborate our findings on the relationships between Ca^{2+} sparks and STOCs shown in Figs. 1–3, we decided to directly visualize RYRs and BK channels in these cells as addressed below.

RYR1 and RYR2 are the major isoforms, and both of them form puncta in ASM

ASM cells from rat express multiple isoforms of RYRs (Du et al., 2005). As a first step to address the spatial relationship between BK channels and RYRs, we identified the RYR isoforms in ASM from mice. Using primers specific for each isoform of RYR, all three of RYR mRNA from de-epithelial tracheal tissues (Fig. 4 A) were detected by reverse transcription PCR. It appears there is only a small amount of mRNA for RYR3 in these cells. The lower abundance of this isoform of

Published July 11, 2011

RYR cannot be attributed to the primer specificity because RYR3 was readily detected in hippocampus from the same mouse (Fig. 4 A).

To determine the subcellular localization of the three RYR isoforms, we performed immunocytochemistry with specific anti-RYRs in single isolated ASM cells. Consistent with the low level of mRNA, RYR3 proteins were weakly expressed in these cells. Moreover, most of RYR3 localized near the nuclei, far away from plasma membrane (Fig. 4 B; also see the 3-D Video 1). In contrast, both RYR1 and RYR2 localized at the periphery of the cells, and their quantities decreased further into the center of the cells (Fig. 4 B and Videos 2 and 3). Another feature of these two isoforms is that both of them distribute nonhomogeneously and form puncta. The mean sizes of puncta were 6.5 ± 0.5 voxels for RYR1 and 8.2 ± 0.7 for RYR2 (n = 5 cells for RYR1 and n = 7 cells for RYR2, P < 0.09, RYR1 vs. RYR2). Given the voxel size of the images, the maximal plasma membrane area covered by each punctum on average was 0.05–0.160 μm^2 for RYR1 and 0.06–0.18 μm^2 for RYR2 (see Materials and methods for calculation). Based on the results of reverse transcription PCR and immunocytochemistry, we conclude that (a) RYR3 is present, but at lower abundance and further inside the cells, especially in the perinuclei regions, and (b) RYR1 and RYR2 represent the major forms of RYRs and form puncta in these cells.

Only a small portion of RYR1/RYR2 and BK channels colocalize

Because RYR1 and RYR2 are the dominant isoforms localized beneath the plasma membrane in a punctuate manner, we determined whether BK channels colocalize with these two types of RYRs by carrying out dual immunocytochemistry. Fig. 5 A displays an example showing the distribution and spatial relationship of RYR2 and BK channels. Two striking features stand out in their distributions. (1) Similar to RYRs, BK channels form puncta along the membrane (Video 4). The size of BK channel puncta was 11 ± 0.7 voxels, which could possess a plasma membrane area of 0.07–0.22 μm^2 (see Materials and methods for calculation). (2) Only a small subset of RYRs and BK channels colocalized near the surface membrane. Quantitatively, <0.2% of RYR1 and RYR2 puncta colocalized with BK channels (Fig. 5 B) in the whole cell based on the estimate of the distance between the centers of RYRs and BK channel puncta. (When the nearest voxel distances between these channel puncta were considered, 9% of RYR2 puncta and 20% of RYR1 puncta were colocalized with BK channel puncta.) On average, the center of mass distance between RYR1s and their closest neighboring BK channel punctum was 296 ± 8.8 nm (n = 5 cells, 692 RYR1 puncta), and the center between RYR2s and their closest neighboring BK channel punctum was 340 ± 7 nm (n = 6 cells, 862 RYR2 puncta). A one-way ANOVA test indicated that BK channels localize further from RYR2s compared with RYR1s (P = 0.0006). The distribution of the center of mass distance between RYRs and BK channel puncta can be fitted with the probability distribution of distance to closest random point (Fig. 5 B). This fitting suggests that BK channel puncta randomly distribute inside the microdomain of Ca^{2+} sparks.

One Ca^{2+} spark activates multiple puncta of BK channels to generate a STOC

To determine the number of BK channel puncta that could be activated by an RYR punctum, we performed

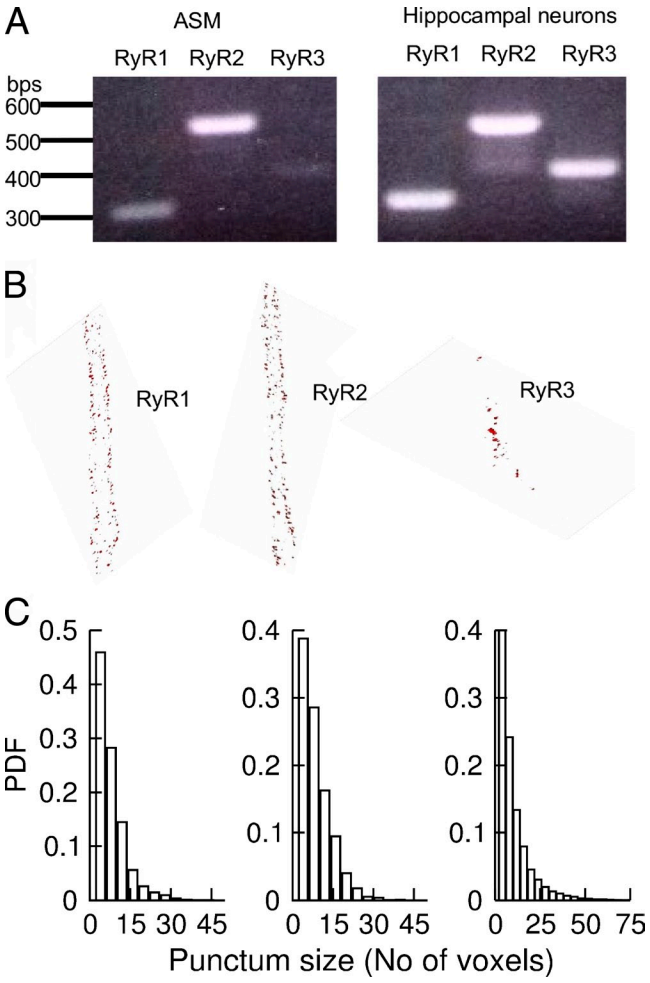

Figure 4. Type and distribution of RYRs in mouse ASM. (A) Reverse transcription PCR detected mRNA for three types of RYRs in ASM (left) and hippocampus (right). (B) RYR1 and RYR2 localize near the plasma membrane, whereas RYR3 localizes near the nucleus. The images show the localization of three types of RYRs in a 3-D projection of 1-μm thickness in the middle of the cells. The distribution of RYRs through the whole cells can be viewed in Videos 1–4. Pixel size in x and y is 80 nm, and the z spacing is 250 nm. (C) Histograms of RYR puncta. The mean size and SEM of puncta were 6.5 ± 0.5 voxels for RYR1 (n = 5 cells), 8.2 ± 0.7 voxels for RYR2 (n = 7 cells), and 13.0 ± 1.4 voxels (n = 5) for RYR3. P < 0.09, RYR1 versus RYR2; P < 0.002, RYR1 versus RYR3; P < 0.006, RYR2 versus RYR3; unpaired t test after ANOVA. PDF, probability density function.

Published July 11, 2011

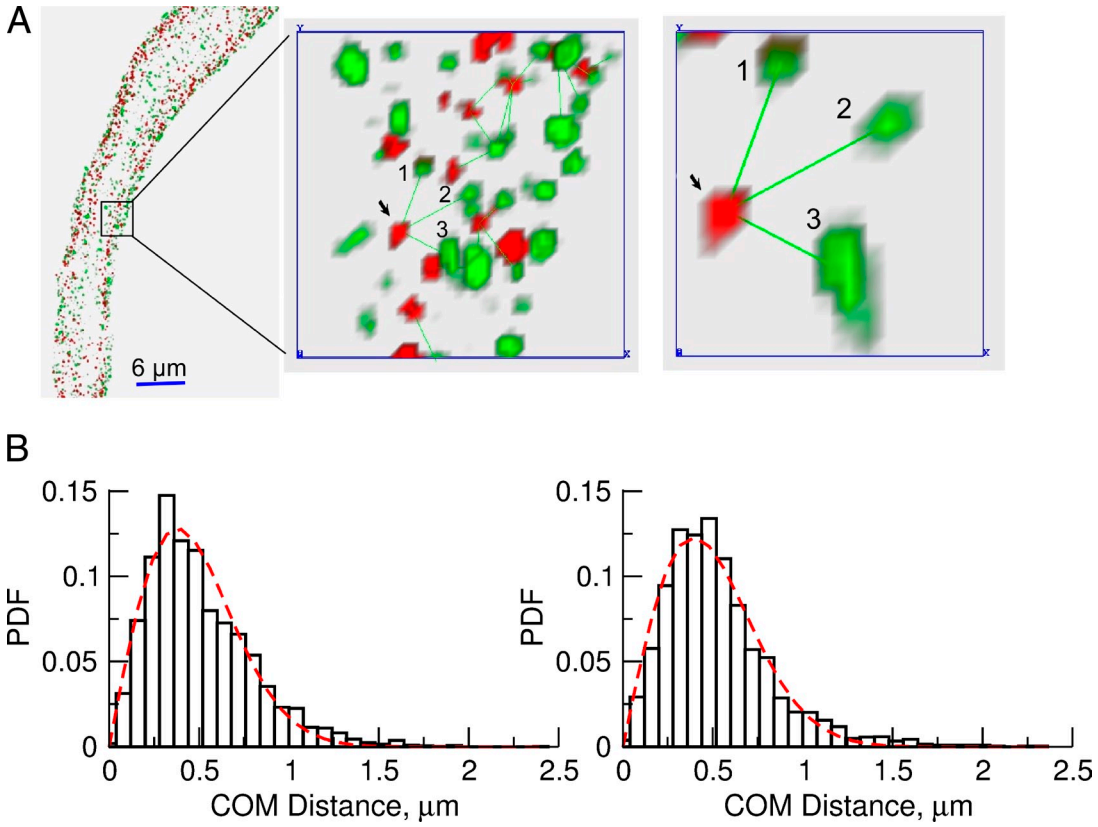

Figure 5. Spatial relationship between RYRs and BK channels. (A) A representative immunostaining showing the spatial relationship between RYR2s and BK channels in approximately one third of the length of a cell. The anti-BK antibody was labeled with Alexa Fluor 488 and is pseudocolored green, and the anti-RYR antibody was labeled with Alexa Fluor 594 and is pseudocolored red. The images show the projection of BK channels and RYR2s localized within 720 nm from the surface membrane. The first inset is the expanded view of RYR2 and BK channels in the box region. Green lines connect RYR2 puncta to BK channels within 600 nm. The right inset depicts the relationship between an RYR2 punctum, as marked by the arrow in the first inset, and its nearby BK channel puncta, indicated by numbers. To display this RYR2 punctum and its corresponding BK channels, RYR2s and BK channels above and below were removed. The center to center distances between the RYR2 punctum and the BK channel puncta are 432 nm (1), 560 nm (2), and 598 nm (3). These distances were used to simulate I_{BK}s shown in Fig. 7 and Fig. S3. (B) Histograms of the center of mass (COM) distance between RYR1 puncta and the closest BK channel puncta (left) and between RYR2 puncta and the closest BK channel puncta (right). Surprisingly, most BK channel puncta do not colocalize with either RYR1 puncta or RYR2 puncta. Dashed lines are the best fits of the probability distribution of distance to the closest random point. The fitting function is $y = 2\pi \times D \times x \times \exp(-\pi D x^2)$, where D is the puncta density (puncta/micrometers squared),and x is the distance (in micrometers; see eq. 8.2.9 in Cressie, 1993). From the fitting, it yields 1.11 puncta/μm^2 for RYR1 and 1.02 puncta/μm^2 for RYR2. This is not the density on the entire plasma membrane, but rather the density on the membrane near each RYR.

the following analysis. First, we derived the spatial-temporal $[Ca^{2+}]$ profile resulting from a mean measured $I_{Ca(spark)}$ (Fig. 1; Bao et al., 2008). We used the $[Ca^{2+}]$ profile at the peak of $I_{Ca(spark)}$ (i.e., 9 ms, which represents the highest $[Ca^{2+}]$ being reached during Ca^{2+} sparks; see Materials and methods section Simulation of the spatial-temporal profile . . . and Fig. 7 B in Bao et al., 2008). From this $[Ca^{2+}]$ spatial function, we then calculated the BK P_o as a function of the distance (at 0 mV) from the center of the given RYR punctum to the center of its closest neighboring BK channel punctum (see Materials and methods). As shown in Fig. 6 A, at 0 mV, a BK channel localized <300 nm from the center of an RYR punctum would be activated at a P_o of 1, and its P_o decreases steeply as BK channels localize further away; this P_o reaches almost zero when the distance is ~600 nm. A count of the number of BK puncta within 600 nm of an RYR puncta revealed that ~20% of RYR1 and RYR2 did not have an associated BK channel punctum, and <5% of RYRs had >10 BK channel puncta. On average, an RYR2 punctum had 1.7 ± 0.05 BK channel puncta within 600 nm, and an RYR1 punctum had 2.5 ± 0.1 BK channel puncta nearby ($n = 5$ cells for RYR1 and 6 cells for RYR2, $P < 0.001$ RYR1 vs. RYR2 with a one-way ANOVA).

By applying $P_o(d)$ to the spatial relationship between BK channel puncta and RYR puncta (Fig. 5 B), we finally arrived at a relationship between an RYR punctum and the number of BK channel puncta being activated (Fig. 6, B and C). Because the P_o of each BK punctum depends on its distance from the RYR, we calculated the number of activated BK channel puncta by weighting each nearby BK channel punctum by its P_o, as shown by

Published July 11, 2011

the red lines in Fig. 6 (B and C; see the legend for calculation). With this calculation, on average, an RYR2 punctum activated 1.26 ± 0.04 BK channel puncta, and an RYR1 punctum activated 1.92 ± 0.07 BK channel puncta (n = 5 cells for RYR1 and 6 cells for RYR2).

Because ASM cells have a resting potential of ∼40 mV, we further estimated the number of BK channel puncta activated by RYRs at this physiological potential by the same technique, but using a P_o appropriate for −40 mV. Fig. 6 (B and C, green lines) shows that ∼40–50% of RYR1 and RYR2 did not have an associated BK channel punctum at this potential. On average, an RYR2 punctum activated 0.78 ± 0.03 BK channel puncta, and an RYR1 punctum activated 1.25 ± 0.05 BK channel puncta (n = 5 cells for RYR1 and 6 cells for RYR2). These estimates suggest that although the physical relationship between RYRs and BK channels in a spark microdomain does not change at different potentials, the functional size of a spark microdomain becomes smaller as the potentials become more negative.

Both RYR and BK puncta contain multiple channels

The distribution of BK channel puncta that can be activated by Ca^{2+} sparks (Fig. 6) also provides evidence that the average punctum consists of multiple BK channels based on the following calculation. Mean STOC amplitude at 0 mV (E_k = −80 mV) was 95 ± 14 pA (n = 28 cells). This current could result from the opening of ∼15 BK channels, assuming a unitary conductance of 80 pS under the K^+ gradient used in this study. Because one Ca^{2+} spark could activate only ∼50% of BK channels in two to three puncta, each punctum could be made up of 10–15 BK channels.

Do RYR puncta consist of one RYR or multiple RYRs? To address this question, we first estimated the number of RYRs responsible for a Ca^{2+} spark. Using the signal mass approach, we estimated that $I_{Ca(spark)}$ has a peak amplitude of 2.8 pA (Fig. 1 B, c). Because under pseudo-physiological conditions RYR has a unitary current of ∼0.35 pA (Mejía-Alvarez et al., 1999), 2.8 pA $I_{Ca(spark)}$ could result from the opening of at least eight RYRs. We next examined whether a Ca^{2+} spark is the result of the activity of RYRs in one punctum or multiple puncta by testing whether RYRs in a punctum can activate RYRs in its closest neighboring punctum. We found that the distances between these RYRs are 0.6 ± 0.06 µm for both RYR1 and RYR2. Given that at steady-state $[Ca^{2+}]$, RYR1 and RYR2 have an EC_{50} of ∼1 µM (Fill and Copello, 2002; Laver, 2007), the probability that activation of RYRs in one punctum leads to the activation of RYRs in a neighboring punctum should be <0.5 because the maximal $[Ca^{2+}]$ at 600 nm from the sparks reaches approximately ≤2 µM (see Fig. 7 in Bao et al., 2008). Also, spontaneous Ca^{2+} transients always appear in the form of Ca^{2+} sparks but not in the form of regional or global changes in these cells (Fig. 1; ZhuGe et al., 1998; Bao et al., 2008). Therefore, we conclude that Ca^{2+} sparks result from the opening of RYRs in a single punctum rather than multiple puncta, and so a single RYR punctum consists of multiple RYRs.

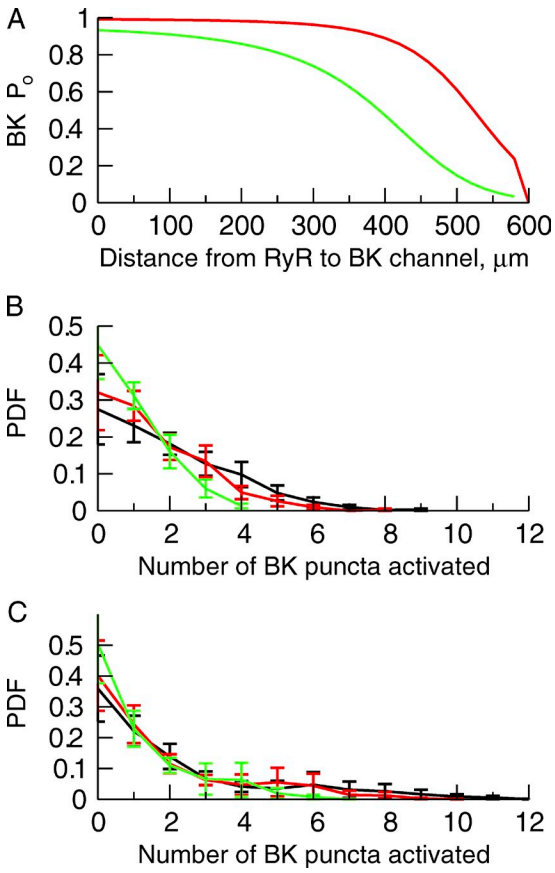

Figure 6. A Ca^{2+} spark activates multiple clusters of BK channels to generate a STOC. (A) Calculated P_o of a BK channel at 0 mV (red line) and −40 mV (green line) as a function of distance from the spark. Combining eq. 14 from Bao and Cox (2005) for the $P_{o,ss}$ ($[Ca^{2+}]$,V) and reaction-diffusion simulations of sparks that yield free $[Ca^{2+}]$(d,t) allows the calculation of $P_{o,ss}$(d) (setting t = 9 ms, the peak of $I_{Ca(spark)}$). (B and C) Probability distribution of the number of BK channel clusters activated by RYR2 (B) and RYR1 (C) puncta. The function in A was applied to the spatial relationship between RYRs and BK channels as shown in Fig. 5 to derive the number of BK channel puncta being activated. Black lines are the count of the number of puncta within 600 nm. Red lines and green lines are the expected numbers of BK clusters activated at 0 mV and −40 mV, respectively, by weighting each nearby BK cluster by its P_o. The expected value is $\Sigma_i(P_{o,i})$, where $P_{o,i}$ is the P_o of the i-th BK cluster within 600 nm of the RYR. Error bars represent means ± SEM. PDF, probability density function.

A mathematical model predicts STOCs

To mathematically model STOCs reliably using the spatial organization of RYRs and BK channels derived from immunostaining experiments, we validated BK channel current kinetics in response to a $[Ca^{2+}]$ jump. To do so, we first derived functions describing the activation and deactivation time constants of the BK channel using the results from $[Ca^{2+}]$ jump experiments performed by

Published July 11, 2011

Markwardt and Isenberg (1992) in urinary bladder myocytes (the only study of this sort in smooth muscle). We defined that (a) τ_{decay} = 0 0.025 × exp(E/50 mV), where E is voltage, and (b) τ_{act} = mE + b, with both m and b being interpolations between the slope and intercepts, respectively, as seen in Fig. 9 in Markwardt and Isenberg (1992) for the low and high [Ca^{2+}] curves (e.g., at low [Ca^{2+}] we used the m and b values from their low [Ca^{2+}] curve). We then applied these functions to drive the BK channel P_o toward the steady-state $P_{o,ss}$ in response to each [Ca^{2+}] jump (see Materials and methods). Fig. S1 A displays the time course of BK channel currents caused by a step to 6 µM [Ca^{2+}] at three different voltages, and Fig. S1 B shows the activation and decay constants of BK channel currents as a function of voltage and [Ca^{2+}]. A comparison between these simulations and Fig. 9 in Markwardt and Isenberg (1992) confirmed that the model of BK channels we used can reliably replicate the BK channel behavior observed in the experiments in smooth muscle. For example, upon a step to 6 µM Ca^{2+} from 0 µM Ca^{2+}, τ_{act} is 29.3 ms in the simulation and ~23 ms in the experimental data; upon stepping back to 0 µM Ca^{2+}, τ_{decay} is 25 ms in the simulation and ~25 ms in the experimental data.

Having validated the BK channel model, we simulated STOCs using the spatial relationship between each RYR and its nearby BK channels as identified experimentally (Fig. 5). Each BK cluster was assigned to have 10 channels (see previous section) and exposed to the appropriate spatio-temporal profile of [Ca^{2+}] derived from a reaction-diffusion spark simulation (Bao et al., 2008) based on estimated mean $I_{Ca(spark)}$ (i.e., an amplitude of 3.36 pA with a 9-ms rise time and a 12-ms τ_{decay}). Dictated by their distance to RYRs, each BK channel cluster gives rise to a unique time course of I_{BK}. Fig. 7 A displays I_{BK}s from each BK channel cluster as if they were recorded at 0 mV when exposed to a Ca^{2+} spark that results from the opening of RYRs marked in the insets of Fig. 5 A. By summing I_{BK} from all BK channel clusters that can be activated by this RYR2 cluster, we obtained a STOC with an amplitude of 35 pA, a TTOD of 22 ms, and a τ_{decay} of 31 ms. On average, simulated STOCs had an amplitude of 114 ± 15.3 pA, with a TTOD of 22.9 ± 3.2 ms and a τ_{decay} of 38 ± 5.8 ms (n = 6 cells and 862 pairs of RYR2 and BK channels; Fig. 7 B). When held at 0 mV, these cells generated STOCs with an amplitude of 95 ± 14 pA, a TTOD of 29.4 ± 2.7 ms, and a τ_{decay} of 34.9 ± 3.4 ms (n = 28 cells). Therefore, simulated STOCs exhibit similar amplitude and kinetics as experimental STOCs in these cells. This conclusion is further strengthened by comparing the effects of varying $I_{Ca(spark)}$s (Fig. S2) and voltage (see following section) on simulated and measured STOCs.

A benefit of the modeling is that the P_o over time of each BK cluster can be calculated. As is evident in Fig. 7 A, the I_{BK} generated by the nearest cluster to the RYRs followed more closely the rise of [Ca^{2+}], with a P_o reaching 0.4 at the plateau. For BK clusters further away from the RYRs, the resultant I_{BK}s rose with a delay compared with the corresponding [Ca^{2+}], and the P_o of these channels reached only ~0.2 and 0.1.

A more careful examination of the temporal relationships between I_{BK}s and their corresponding [Ca^{2+}]

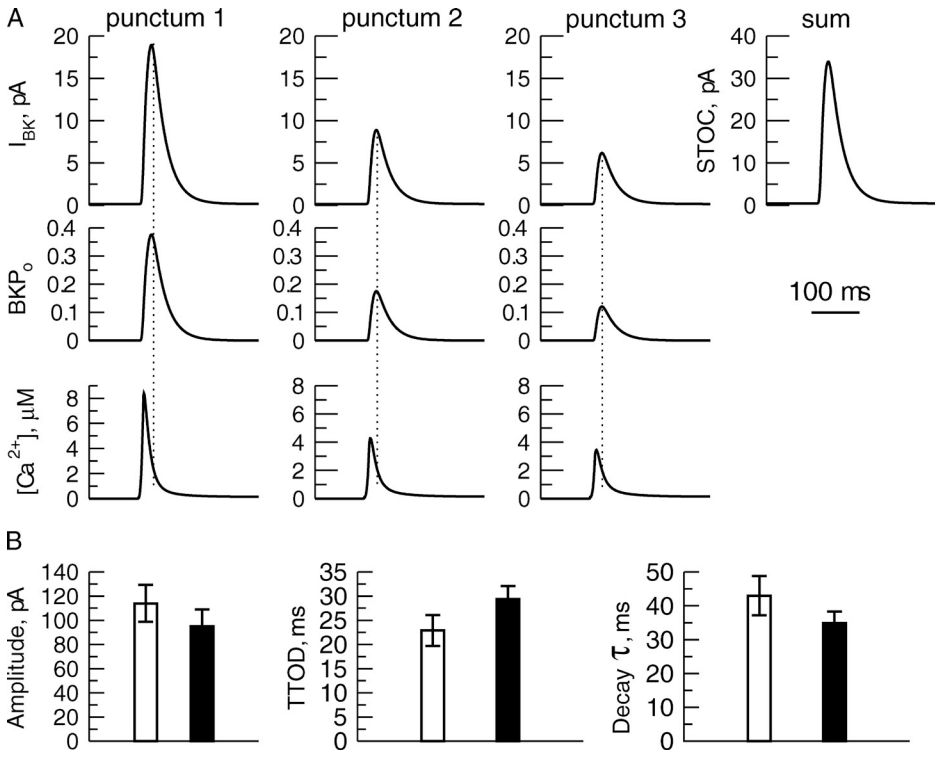

Figure 7. Simulated STOCs recapitulate the salient feature of STOCs recorded experimentally. (A) The time course of I_{BK}s (top) generated by each BK channel punctum as marked in Fig. 5 and the underlying [Ca^{2+}] (bottom) as a result of a Ca^{2+} spark with an average $I_{Ca(spark)}$ (see Materials and methods). The middle row shows the corresponding P_o of BK channels in each punctum. E_k is −80 mV, and the holding potential is 0 mV. The three dotted lines mark the onset of I_{BK} decay. The far right trace in the top row is the STOC created by adding the I_{BK}s from the three puncta near this RYR2 punctum. (B) The parameters of simulated STOCs (open bars) activated by RYR2s resemble those from measured STOCs (closed bars). Simulated STOCs were obtained based on the spatial relationship between RYR2 and BK channels as shown in Fig. 5, and experimental STOCs were measured at 0 mV (E_k, −80 mV). Data are means ± SEM.

Published July 11, 2011

revealed that I_{BK}s began to decay at the time when [Ca^{2+}] decreased to 2 µM (Fig. 7 A). This value is lower than the EC_{50} of BK channels to Ca^{2+}, which is 3.5 µM in smooth muscle (Tanaka et al., 1997).

Simulated STOCs recapitulate the voltage dependence of STOCs recorded experimentally

To further evaluate the mathematical model of sparks and STOCs, we compared the voltage dependence of STOCs acquired in experiments to simulated STOCs. This is necessary and of physiological significance given that ASM cells possess a resting potential of around −40 mV, and upon stimulation under normal conditions their potential does not reach 0 mV (a potential set in the other experiments in this study to prevent STICs). To determine the voltage dependence of STOCs, we used the same paradigm as we developed for gastric smooth muscle (ZhuGe et al., 2002). In this paradigm, we set the E_k to −28 mV to facilitate the detection of STOCs at very negative potentials, and 50 µM niflumic acid was added to block STICs (Hogg et al., 1994; Janssen and Sims, 1994). Fig. 8 A (left) displays a representative set of recordings of STOCs when the cell was clamped between −100 and 20 mV. Simply considering the driving force at each potential, we can calculate the conductance underlying STOC ($G_{(STOC)}$) for each event and obtain the relationship between $G_{(STOC)}$ and voltage (Fig. 8 B). Consistent with our observations in gastric smooth muscle cells (ZhuGe et al., 2002), $G_{(STOC)}$ increased as the voltage became less negative. We further analyzed the relationship between STOC τ_{decay} and voltage and between $TTOD_{STOC}$ and voltage. Interestingly, STOC τ_{decay} increased as the voltage became less negative, but the $TTOD_{STOC}$ was flat across the voltages examined in ASM cells (Fig. 8, B and C).

To simulate the voltage dependence of STOCs using the measured spatial relationship between BK channels and RYRs, we performed STOC simulations clamped at the different voltages. Fig. S3 displays the time course of P_o for each BK punctum marked in Fig. 5 A at different voltages. Using the same calculation as in Fig. 7 A, we can estimate STOCs for that RYR2 cluster at each voltage. Fig. 8 A shows STOC events at different voltages from 25 RYR2 clusters. Fig. 8 (B and C) displays the relationship of three STOC parameters to voltage from 862 pairs of RYR2s and BK channels from six cells. Strikingly, all of the three aforementioned parameters in simulated STOCs show the same relationship to the voltage as STOCs recorded experimentally.

DISCUSSION

In this study, using a combination of functional and immunocytochemical analyses, we uncovered the spatial arrangements of RYRs and BK channels that underlie the activation of STOCs by Ca^{2+} sparks in ASM cells. We found that both RYRs and BK channels distribute in the

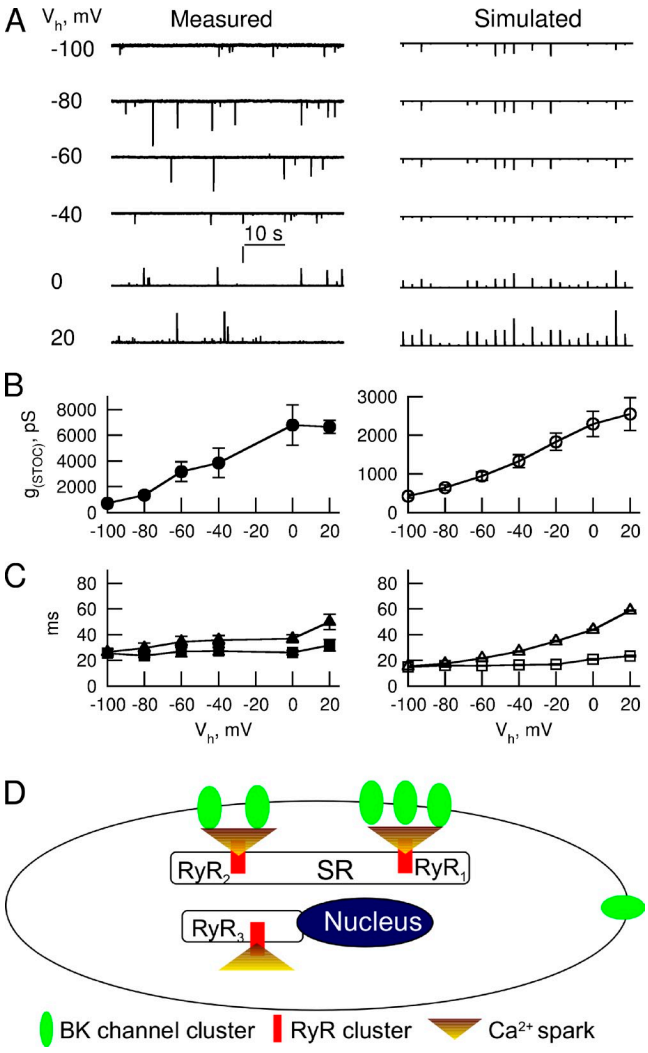

Figure 8. Voltage dependence of measured STOCs and simulated STOCs. To record and measure STOCs at large negative potentials, E_K was set at −28 mV. (A, left) Traces exhibit STOCs recorded at different holding potentials (V_h). Vertical bar, 25 pA for the V_hs between –100 and –40 mV, and 50 pA for all others. (right) Simulated STOCs from 25 RYR2 puncta at the V_hs shown on the left. Note that the vertical bar in the left column also applies to all voltages on the right and represents 25 pA, but the horizontal time bar on the left does not apply to the results on the right (because the temporal spacing between simulated STOCs is arbitrary). (B) Averaged conductance of STOC ($G_{(STOC)}$) as a function of voltage derived from measured (left) and simulated (right) STOCs ($n = 6$ cells for both cases in B and C). (C) $TTOD_{STOC}$ (closed and open squares for experimental and simulated data, respectively) and τ_{decay} (closed and open triangles) as a function of voltage. (D) Spatial organization of RYRs and BK channels in ASM cells. RYR1 and RYR2 clusters localize near the plasma membrane and functionally couple with approximately two to three BK channel clusters to generate STOCs. RYR3 clusters distribute near the nucleus and could activate targets to be determined. BK channels in the plasma membrane outside the Ca^{2+} spark microdomains could be activated by unknown Ca^{2+}-permeable channels. SR, sarcoplasmic reticulum. Error bars represent means ± SEM.

Published July 11, 2011

form of clusters, and the opening of a single cluster of RYRs can act on two to three clusters of BK channels on average that reside randomly in an area within ~600 nm from the RYRs. Integrating this spatial relationship with BK channel kinetics and the spatial-temporal profile of [Ca^{2+}] generated by Ca^{2+} sparks, we can model I_{BK} with characteristic features of STOCs from experiments in the physiological membrane potentials, thus providing a mechanistic understanding of Ca^{2+} spark signaling in smooth muscle.

Spatial organization of RYRs and BK channels in spark-generating sites

In theory, two types of BK channel distributions could result in the generation of STOCs by Ca^{2+} sparks. In one scenario, individual BK channels localize randomly or homogeneously in the surface membrane, independent of RYR location. As a result, only the BK channels that localize within a certain distance of the RYRs could be activated during a spark because [Ca^{2+}] decreases steeply as it moves away from RYRs, the Ca^{2+} source. Alternatively, BK channels could distribute in much higher density near the RYRs, i.e., RYRs and BK channels constitute a physical microdomain. In our previous study of amphibian gastric smooth muscle (ZhuGe et al., 2002), we observed that the conductance of STOCs reaches a plateau at positive potentials, arguing that the alternative scenario could be the structural basis for Ca^{2+} sparks to induce STOCs. In the present study, we directly tested these two possibilities by visualizing BK channels and RYRs using high spatial resolution immunofluorescence microscopy. We found that both RYRs and BK channels distribute in puncta. Our calculation indicates that each punctum represents a group of clustered channels, which is consistent with our previous hypothesis that BK channels concentrate near RYRs (ZhuGe et al., 2002).

However, to our surprise, only ~0.2% of BK channel clusters colocalize with RYR clusters (Fig. 5 B). This result alone suggests that a physical coupling between RYRs and BK channels is not required for Ca^{2+} sparks to generate STOCs. Interestingly, the distance distribution from RYR clusters to their closest BK channel clusters (Fig. 5 B) suggests that a Ca^{2+} spark could act on multiple BK channel clusters to give rise to a STOC. Several lines of evidence indeed indicate that this is the case. First, Ca^{2+} sparks generate a Ca^{2+} microdomain with an area of ~500 nm in radius within which [Ca^{2+}] is >3.5 µM (Bao et al., 2008). Second, within such a Ca^{2+} microdomain, the BK channel can be activated with a P_o of 0.5 in smooth muscle and in our model (Fig. 6; Tanaka et al., 1997). Third, within the Ca^{2+} microdomain, there are, on average, two to three BK channel clusters. With these new results, we propose that a Ca^{2+} spark site is composed of a single cluster of RYRs and a variable number of clustered BK channels (Fig. 8 D). Considering that the distribution of the distance between RYR clusters and the closest BK channel clusters can be fit with the probability distribution of distance to the closest random point (Fig. 5 B), we suggest that BK channel clusters randomly distribute inside the Ca^{2+} spark microdomains (note that they are not randomly distributed along the entire plasma membrane). Our findings on the spatial arrangement of BK channels and RYR are not only significant for understanding the activation of STOCs by Ca^{2+} sparks, but they also raise new possibilities for further exploration. For instance, it would be interesting to investigate what determines the number of channels in a cluster and cluster density and whether BK channels form clusters as a result of the involvement of scaffolding proteins or localize in specialized structural domains such as caveolae or lipid rafts in the plasma membrane (Shmygol et al., 2007; Lu et al., 2010).

The factors affecting STOC amplitude and kinetics

A common observation on STOCs from different smooth muscles is that there is a great variation in the amplitude of STOCs (Benham and Bolton, 1986; Nelson et al., 1995; Bolton and Imaizumi, 1996; ZhuGe et al., 1998; Pérez et al., 1999; Kirber et al., 2001; Löhn et al., 2001; Ohi et al., 2001). This is even evident in a single cell as demonstrated in Fig. 2. In the present study, we found that the number of BK channel clusters being activated by Ca^{2+} sparks and BK channel kinetics affect STOC amplitude, and, thus, these two parameters could contribute to the variation in STOC amplitude. As shown in Fig. 6, the number of BK channel clusters that can be affected by Ca^{2+} sparks spans from 0 to 15. Assuming each cluster has a fixed number of BK channels that open at the same P_o, Ca^{2+} sparks could produce STOCs with amplitudes that differ by 15-fold (excluding STOC-less events).

The influence of BK channel kinetics on STOC amplitude lies in the fact that BK channel kinetics is a rate-limiting step for STOC activation. As shown in Fig. S1 B, in response to a step function of [Ca^{2+}] between 1 and 320 µM, BK channel currents develop with time constants between 40 and 5 ms at 0 mV. Therefore, if [Ca^{2+}] near the BK channels dissipates before their activations reach the steady state, the STOC amplitude would be smaller than its maximal (i.e., steady state) value. Longer duration sparks allow BK channels more time to reach their steady-state P_o and therefore could produce a bigger STOC. This is proportionally a larger effect on BK channels further from the spark (but still <600 nm away at 0 mV) because the lower [Ca^{2+}] there causes them to have a slower activation rate. However, in absolute terms, it may not be as important because, if far enough away, the steady-state P_o may be small, and thus the BK cluster wouldn't contribute much to the total STOC.

The kinetics of BK channels affects not only the amplitude of STOCs but also the rise time of STOCs. In this study, we found that signal mass rise time shows no

Published July 11, 2011

difference compared with $TTOD_{STOC}$ (Fig. 1). Because signal mass is an integrated amount of Ca^{2+} being released during Ca^{2+} sparks, its value should continue to increase as long as RYRs in the spark site are open. The similarity between signal mass rise time and $TTOD_{STOC}$ suggests that the kinetics of the BK channel plays a role in determining the duration of STOC rise. On the other hand, it suggests that the open time of RYRs in the spark sites is another critical variable affecting the rise time of a STOC.

What, then, determines the decay of STOCs? Our data support the notion that the kinetics of BK channels is the dominant factor in smooth muscle. First, STOCs in ASM can be fitted well with a single exponential function with a time constant similar to the mean open time of BK channels. Second, the time constants are independent of both amplitudes of STOCs and Ca^{2+} sparks. With computer modeling of STOCs that includes the spatial relationship between RYRs and BK channels, we observed that the $[Ca^{2+}]$ near the BK channels drops rapidly to the level below the EC_{50} (3.5 µM at 0 mV) when a Ca^{2+} spark terminates. The underlying reasons why BK channel kinetics determines STOC decay are that (a) RYRs and BK channels are close, though not physically associated, and (b) the Ca^{2+} sensitivity of BK channels is sufficiently low (Singer and Walsh, 1987; Tanaka et al., 1997; Bao and Cox, 2005).

The types of RYRs that functionally couple with BK channels to generate STOCs

Consistent with the findings in a variety of smooth muscles (Du et al., 2005; Yang et al., 2005; Essin and Gollasch, 2009; Yang et al., 2009; Clark et al., 2010), we detected all three types of RYRs at mRNA and protein levels in mouse ASM. As a result, an intriguing question arises as to the types of RYRs that functionally couple with BK channels. Our immunostaining results show that both RYR1 and RYR2 localize close to the plasma membrane and thus are well positioned to be responsible for the generation of STOCs. Interestingly, RYR3s concentrate in the perinuclear region, and Ca^{2+} release by an individual RYR3 cluster is therefore unable to activate BK channels in the plasma membrane. Therefore, we can conclude that RYR3 does not couple with BK channels to generate STOCs.

Localization of RYR1 and RYR2 near the plasma membrane raises the question of whether both channels couple with the same population of BK channels. Two lines of evidence indicate that RYR1s and RYR2s could activate different clusters of BK channels. First, the distance between RYR1s and their closest BK channel cluster is shorter than that between RYR2 and BK channels. Second, the numbers of BK channels that can be activated by RYR1s is more than that by RYR2s. Therefore, our results suggest that RYR1s and RYR2s could constitute independent Ca^{2+} spark microdomains (Fig. 8 D).

In addition to the findings in ASM, previous studies by us and others revealed that RYR3 also localizes in perinuclear regions in vascular smooth muscle and chromaffin cells (ZhuGe et al., 2006; Clark et al., 2010). These findings suggested RYR3s could mediate specific unknown functions (Fig. 8 D). It is worth mentioning that in vascular smooth muscle cells without RYR3, the frequency and amplitude of STOCs are increased (Löhn et al., 2001). The authors suggest that under physiological conditions, these channels exert negative influence on RYR1/2, whose activation produces Ca^{2+} sparks. Furthermore, the authors proposed three possible mechanisms to account for this inhibition: (1) Ca^{2+} released from RYR3s inhibits either RYR1 or RYR2; (2) inactivation of VDCC that provides initial Ca^{2+} influx to trigger Ca^{2+} sparks; and (3) depletion of Ca^{2+} stores from which Ca^{2+} sparks occur. Given the distinctive distribution patterns of RYR1/2 and RYR3, it appears the first two mechanisms cannot account for the inhibition because a close proximity between RYR1/2 and RYR3 and between VDCC and RYR3 is required for these mechanisms to operate. If RYR1/2 and RYR3 share the same Ca^{2+} stores, the third mechanism could be possible. However, the authors did not observe any difference in Ca^{2+} spark amplitude between wild-type and $RYR3^{-/-}$ cells. Therefore, our results on the distribution of the three types of RYRs raise other possibilities for the inhibition that warrant further investigation.

Role of BK clusters far away from RYRs

An unexpected finding in this study is that >50% of BK channels localized far away from RYRs so that they could not be the targets of RYRs (64.5 ± 6.2% of BK channels outside of RYR1 domains [n = 5 cells] and 65.2 ± 6.9% of BK channels outside of the RYR2 domains [n = 6 cells]). This suggests that in addition to Ca^{2+} sparks, other forms of Ca^{2+} signals could activate BK channels (Fig. 8 D). In fact, several Ca^{2+} sources have been demonstrated or proposed to activate BK channels. In portal vein and cerebral artery smooth muscle cells, Ca^{2+} from inositol trisphosphate receptors can activate STOCs (though it has yet to be determined whether underlying Ca^{2+} events are Ca^{2+} pufflike local Ca^{2+} signals; Kitamura et al., 1992; Zhao et al., 2010). In vascular smooth muscle and ASM, VDCCs could activate BK channels either as the form of STOCs or whole-cell I_{BK} (Wang et al., 1997; Guia et al., 1999). Finally, nonselective Ca^{2+} channels can directly or indirectly open BK channels (Zou et al., 2002). More experiments are needed to elucidate the activation mechanism and role of BK channels outside the Ca^{2+} spark microdomains in smooth muscle.

In summary, in this study, by combining functional analysis, immunocytochemistry, and computer modeling, we uncover the molecular basis and mechanism underlying the activation of STOCs by Ca^{2+} sparks. Because uncoupling of Ca^{2+} sparks and STOCs contributes

to disorders such as hypertension, overactive bladder, and retinopathy, the results and approaches presented in this study could be useful in understanding these disorders and local Ca^{2+} signaling in general.

We wish to thank Rongfeng Bao for technical assistance in cell isolation and Valerie Decrescenzo and John Walsh for stimulating discussions.

This study was supported by grants from the National Institutes of Health (HL73875), American Heart Association, Charles Hood Foundation, and British Heart Foundation and Telethon (GGP08153).

Edward N. Pugh Jr. served as editor.

Submitted: 4 March 2011
Accepted: 22 June 2011

REFERENCES

Amberg, G.C., A.D. Bonev, C.F. Rossow, M.T. Nelson, and L.F. Santana. 2003. Modulation of the molecular composition of large conductance, Ca(2+) activated K(+) channels in vascular smooth muscle during hypertension. *J. Clin. Invest.* 112:717–724.

Bao, L., and D.H. Cox. 2005. Gating and ionic currents reveal how the BK_{Ca} channel's Ca^{2+} sensitivity is enhanced by its β1 subunit. *J. Gen. Physiol.* 126:393–412. doi:10.1085/jgp.200509346

Bao, R., L.M. Lifshitz, R.A. Tuft, K. Bellvé, K.E. Fogarty, and R. ZhuGe. 2008. A close association of RyRs with highly dense clusters of Ca^{2+}-activated Cl^- channels underlies the activation of STICs by Ca^{2+} sparks in mouse airway smooth muscle. *J. Gen. Physiol.* 132:145–160. doi:10.1085/jgp.200709933

Benham, C.D., and T.B. Bolton. 1986. Spontaneous transient outward currents in single visceral and vascular smooth muscle cells of the rabbit. *J. Physiol.* 381:385–406.

Berridge, M.J., M.D. Bootman, and H.L. Roderick. 2003. Calcium signalling: dynamics, homeostasis and remodelling. *Nat. Rev. Mol. Cell Biol.* 4:517–529. doi:10.1038/nrm1155

Bolton, T.B., and Y. Imaizumi. 1996. Spontaneous transient outward currents in smooth muscle cells. *Cell Calcium.* 20:141–152. doi:10.1016/S0143-4160(96)90103-7

Brainard, A.M., A.J. Miller, J.R. Martens, and S.K. England. 2005. Maxi-K channels localize to caveolae in human myometrium: a role for an actin-channel-caveolin complex in the regulation of myometrial smooth muscle K+ current. *Am. J. Physiol. Cell Physiol.* 289:C49–C57. doi:10.1152/ajpcell.00399.2004

Brenner, R., G.J. Peréz, A.D. Bonev, D.M. Eckman, J.C. Kosek, S.W. Wiler, A.J. Patterson, M.T. Nelson, and R.W. Aldrich. 2000. Vasoregulation by the beta1 subunit of the calcium-activated potassium channel. *Nature.* 407:870–876. doi:10.1038/35038011

Brown, D.A., A. Constanti, and P.R. Adams. 1983. Ca-activated potassium current in vertebrate sympathetic neurons. *Cell Calcium.* 4:407–420. doi:10.1016/0143-4160(83)90017-9

Burdyga, T., and S. Wray. 2005. Action potential refractory period in ureter smooth muscle is set by Ca sparks and BK channels. *Nature.* 436:559–562. doi:10.1038/nature03834

Carrington, W.A., R.M. Lynch, E.D. Moore, G. Isenberg, K.E. Fogarty, and F.S. Fay. 1995. Superresolution three-dimensional images of fluorescence in cells with minimal light exposure. *Science.* 268:1483–1487. doi:10.1126/science.7770772

Clark, J.H., N.P. Kinnear, S. Kalujnaia, G. Cramb, S. Fleischer, L.H. Jeyakumar, F. Wuytack, and A.M. Evans. 2010. Identification of functionally segregated sarcoplasmic reticulum calcium stores in pulmonary arterial smooth muscle. *J. Biol. Chem.* 285:13542–13549. doi:10.1074/jbc.M110.101485

Cressie, N.A. 1993. Statistics for Spatial Data. Revised edition. John Wiley & Sons Inc., New York. 900 pp.

Du, W., J.A. Stiber, P.B. Rosenberg, G. Meissner, and J.P. Eu. 2005. Ryanodine receptors in muscarinic receptor-mediated bronchoconstriction. *J. Biol. Chem.* 280:26287–26294. doi:10.1074/jbc.M502905200

Ermentrout, B. 2002. Simulating, Analyzing, and Animating Dynamical Systems: a Guide to XPPAUT for Researchers and Students. Society for Industrial and Applied Mathematics, Philadelphia. 290 pp.

Essin, K., and M. Gollasch. 2009. Role of ryanodine receptor subtypes in initiation and formation of calcium sparks in arterial smooth muscle: comparison with striated muscle. *J. Biomed. Biotechnol.* doi:10.1155/2009/135249. doi:10.1155/2009/135249

Fill, M., and J.A. Copello. 2002. Ryanodine receptor calcium release channels. *Physiol. Rev.* 82:893–922.

Giannini, G., A. Conti, S. Mammarella, M. Scrobogna, and V. Sorrentino. 1995. The ryanodine receptor/calcium channel genes are widely and differentially expressed in murine brain and peripheral tissues. *J. Cell Biol.* 128:893–904. doi:10.1083/jcb.128.5.893

Guia, A., X. Wan, M. Courtemanche, and N. Leblanc. 1999. Local Ca2+ entry through L-type Ca2+ channels activates Ca2+-dependent K+ channels in rabbit coronary myocytes. *Circ. Res.* 84:1032–1042.

Harper, A.A., L. Catacuzzeno, C. Trequattrini, A. Petris, and F. Franciolini. 2001. Verapamil block of large-conductance Ca-activated K channels in rat aortic myocytes. *J. Membr. Biol.* 179:103–111. doi:10.1007/s002320010041

Hogg, R.C., Q. Wang, and W.A. Large. 1993. Time course of spontaneous calcium-activated chloride currents in smooth muscle cells from the rabbit portal vein. *J. Physiol.* 464:15–31.

Hogg, R.C., Q. Wang, and W.A. Large. 1994. Action of niflumic acid on evoked and spontaneous calcium-activated chloride and potassium currents in smooth muscle cells from rabbit portal vein. *Br. J. Pharmacol.* 112:977–984.

Janssen, L.J., and S.M. Sims. 1994. Spontaneous transient inward currents and rhythmicity in canine and guinea-pig tracheal smooth muscle cells. *Pflugers Arch.* 427:473–480. doi:10.1007/BF00374263

Karkanis, T., L. DeYoung, G.B. Brock, and S.M. Sims. 2003. Ca2+-activated Cl− channels in corpus cavernosum smooth muscle: a novel mechanism for control of penile erection. *J. Appl. Physiol.* 94:301–313.

Kirber, M.T., E.F. Etter, K.A. Bellve, L.M. Lifshitz, R.A. Tuft, F.S. Fay, J.V. Walsh, and K.E. Fogarty. 2001. Relationship of Ca2+ sparks to STOCs studied with 2D and 3D imaging in feline oesophageal smooth muscle cells. *J. Physiol.* 531:315–327. doi:10.1111/j.1469-7793.2001.0315i.x

Kitamura, K., Z. Xiong, N. Teramoto, and H. Kuriyama. 1992. Roles of inositol trisphosphate and protein kinase C in the spontaneous outward current modulated by calcium release in rabbit portal vein. *Pflugers Arch.* 421:539–551. doi:10.1007/BF00375049

Laver, D.R. 2007. Ca2+ stores regulate ryanodine receptor Ca2+ release channels via luminal and cytosolic Ca2+ sites. *Biophys. J.* 92:3541–3555. doi:10.1529/biophysj.106.099028

Lim, H.H., and C.S. Park. 2005. Identification and functional characterization of ankyrin-repeat family protein ANKRA as a protein interacting with BKCa channel. *Mol. Biol. Cell.* 16:1013–1025. doi:10.1091/mbc.E04-06-0537

Löhn, M., W. Jessner, M. Fürstenau, M. Wellner, V. Sorrentino, H. Haller, F.C. Luft, and M. Gollasch. 2001. Regulation of calcium sparks and spontaneous transient outward currents by RyR3 in arterial vascular smooth muscle cells. *Circ. Res.* 89:1051–1057. doi:10.1161/hh2301.100250

Lu, T., D. Ye, T. He, X.L. Wang, H.L. Wang, and H.C. Lee. 2008. Impaired Ca2+-dependent activation of large-conductance Ca2+-

activated K+ channels in the coronary artery smooth muscle cells of Zucker Diabetic Fatty rats. *Biophys. J.* 95:5165–5177. doi:10.1529/biophysj.108.138339

Lu, T., D.M. Zhang, X.L. Wang, T. He, R.X. Wang, Q. Chai, Z.S. Katusic, and H.C. Lee. 2010. Regulation of coronary arterial BK channels by caveolae-mediated angiotensin II signaling in diabetes mellitus. *Circ. Res.* 106:1164–1173. doi:10.1161/CIRCRESAHA.109.209767

Marhl, M., D. Noble, and E. Roux. 2006. Modeling of molecular and cellular mechanisms involved in Ca2+ signal encoding in airway myocytes. *Cell Biochem. Biophys.* 46:285–302. doi:10.1385/CBB:46:3:285

Markwardt, F., and G. Isenberg. 1992. Gating of maxi K+ channels studied by Ca2+ concentration jumps in excised inside-out multichannel patches (myocytes from guinea pig urinary bladder). *J. Gen. Physiol.* 99:841–862. doi:10.1085/jgp.99.6.841

McGahon, M.K., D.P. Dash, A. Arora, N. Wall, J. Dawicki, D.A. Simpson, C.N. Scholfield, J.G. McGeown, and T.M. Curtis. 2007. Diabetes downregulates large-conductance Ca2+-activated potassium beta 1 channel subunit in retinal arteriolar smooth muscle. *Circ. Res.* 100:703–711. doi:10.1161/01.RES.0000260182.36481.c9

Mejía-Alvarez, R., C. Kettlun, E. Ríos, M. Stern, and M. Fill. 1999. Unitary Ca2+ current through cardiac ryanodine receptor channels under quasi-physiological ionic conditions. *J. Gen. Physiol.* 113:177–186. doi:10.1085/jgp.113.2.177

Meredith, A.L., K.S. Thorneloe, M.E. Werner, M.T. Nelson, and R.W. Aldrich. 2004. Overactive bladder and incontinence in the absence of the BK large conductance Ca2+-activated K+ channel. *J. Biol. Chem.* 279:36746–36752. doi:10.1074/jbc.M405621200

Mitchell, K.J., F.A. Lai, and G.A. Rutter. 2003. Ryanodine receptor type I and nicotinic acid adenine dinucleotide phosphate receptors mediate Ca2+ release from insulin-containing vesicles in living pancreatic beta-cells (MIN6). *J. Biol. Chem.* 278:11057–11064. doi:10.1074/jbc.M210257200

Neher, E. 1998. Vesicle pools and Ca2+ microdomains: new tools for understanding their roles in neurotransmitter release. *Neuron.* 20:389–399. doi:10.1016/S0896-6273(00)80983-6

Nelson, M.T., H. Cheng, M. Rubart, L.F. Santana, A.D. Bonev, H.J. Knot, and W.J. Lederer. 1995. Relaxation of arterial smooth muscle by calcium sparks. *Science.* 270:633–637. doi:10.1126/science.270.5236.633

Ohi, Y., H. Yamamura, N. Nagano, S. Ohya, K. Muraki, M. Watanabe, and Y. Imaizumi. 2001. Local Ca(2+) transients and distribution of BK channels and ryanodine receptors in smooth muscle cells of guinea-pig vas deferens and urinary bladder. *J. Physiol.* 534:313–326. doi:10.1111/j.1469-7793.2001.t01-3-00313.x

Pérez, G.J., A.D. Bonev, J.B. Patlak, and M.T. Nelson. 1999. Functional coupling of ryanodine receptors to K_{Ca} channels in smooth muscle cells from rat cerebral arteries. *J. Gen. Physiol.* 113:229–238. doi:10.1085/jgp.113.2.229

Pérez, G.J., A.D. Bonev, and M.T. Nelson. 2001. Micromolar Ca(2+) from sparks activates Ca(2+)-sensitive K(+) channels in rat cerebral artery smooth muscle. *Am. J. Physiol. Cell Physiol.* 281:C1769–C1775.

Plüger, S., J. Faulhaber, M. Fürstenau, M. Löhn, R. Waldschütz, M. Gollasch, H. Haller, F.C. Luft, H. Ehmke, and O. Pongs. 2000. Mice with disrupted BK channel beta1 subunit gene feature abnormal Ca(2+) spark/STOC coupling and elevated blood pressure. *Circ. Res.* 87:E53–E60.

Samaranayake, H., J.C. Saunders, M.I. Greene, and D.S. Navaratnam. 2004. Ca(2+) and K(+) (BK) channels in chick hair cells are clustered and colocalized with apical-basal and tonotopic gradients. *J. Physiol.* 560:13–20. doi:10.1113/jphysiol.2004.069856

Shmygol, A., K. Noble, and S. Wray. 2007. Depletion of membrane cholesterol eliminates the Ca2+-activated component of outward potassium current and decreases membrane capacitance in rat uterine myocytes. *J. Physiol.* 581:445–456. doi:10.1113/jphysiol.2007.129452

Singer, J.J., and J.V. Walsh Jr. 1987. Characterization of calcium-activated potassium channels in single smooth muscle cells using the patch-clamp technique. *Pflugers Arch.* 408:98–111. doi:10.1007/BF00581337

Tanaka, Y., P. Meera, M. Song, H.G. Knaus, and L. Toro. 1997. Molecular constituents of maxi KCa channels in human coronary smooth muscle: predominant alpha + beta subunit complexes. *J. Physiol.* 502:545–557. doi:10.1111/j.1469-7793.1997.545bj.x

Tunwell, R.E., C. Wickenden, B.M. Bertrand, V.I. Shevchenko, M.B. Walsh, P.D. Allen, and F.A. Lai. 1996. The human cardiac muscle ryanodine receptor-calcium release channel: identification, primary structure and topological analysis. *Biochem. J.* 318:477–487.

Van Helden, D.F. 1993. Pacemaker potentials in lymphatic smooth muscle of the guinea-pig mesentery. *J. Physiol.* 471:465–479.

Wang, Y.X., B.K. Fleischmann, and M.I. Kotlikoff. 1997. Modulation of maxi-K+ channels by voltage-dependent Ca2+ channels and methacholine in single airway myocytes. *Am. J. Physiol.* 272:C1151–C1159.

Yang, X.R., M.J. Lin, K.P. Yip, L.H. Jeyakumar, S. Fleischer, G.P. Leung, and J.S. Sham. 2005. Multiple ryanodine receptor subtypes and heterogeneous ryanodine receptor-gated Ca2+ stores in pulmonary arterial smooth muscle cells. *Am. J. Physiol. Lung Cell. Mol. Physiol.* 289:L338–L348. doi:10.1152/ajplung.00328.2004

Yang, Y., T.V. Murphy, S.R. Ella, T.H. Grayson, R. Haddock, Y.T. Hwang, A.P. Braun, G. Peichun, R.J. Korthuis, M.J. Davis, and M.A. Hill. 2009. Heterogeneity in function of small artery smooth muscle BKCa: involvement of the beta1-subunit. *J. Physiol.* 587:3025–3044. doi:10.1113/jphysiol.2009.169920

Zhao, G., Z.P. Neeb, M.D. Leo, J. Pachuau, A. Adebiyi, K. Ouyang, J. Chen, and J.H. Jaggar. 2010. Type 1 IP_3 receptors activate BK_{Ca} channels via local molecular coupling in arterial smooth muscle cells. *J. Gen. Physiol.* 136:283–291. doi:10.1085/jgp.201010453

ZhuGe, R., S.M. Sims, R.A. Tuft, K.E. Fogarty, and J.V. Walsh Jr. 1998. Ca2+ sparks activate K+ and Cl− channels, resulting in spontaneous transient currents in guinea-pig tracheal myocytes. *J. Physiol.* 513:711–718. doi:10.1111/j.1469-7793.1998.711ba.x

ZhuGe, R., R.A. Tuft, K.E. Fogarty, K. Bellve, F.S. Fay, and J.V. Walsh Jr. 1999. The influence of sarcoplasmic reticulum Ca^{2+} concentration on Ca^{2+} sparks and spontaneous transient outward currents in single smooth muscle cells. *J. Gen. Physiol.* 113:215–228. doi:10.1085/jgp.113.2.215

ZhuGe, R., K.E. Fogarty, R.A. Tuft, L.M. Lifshitz, K. Sayar, and J.V. Walsh Jr. 2000. Dynamics of signaling between Ca^{2+} sparks and Ca^{2+}-activated K^+ channels studied with a novel image-based method for direct intracellular measurement of ryanodine receptor Ca^{2+} current. *J. Gen. Physiol.* 116:845–864. doi:10.1085/jgp.116.6.845

Zhuge, R., K.E. Fogarty, R.A. Tuft, and J.V. Walsh Jr. 2002. Spontaneous transient outward currents arise from microdomains where BK channels are exposed to a mean Ca^{2+} concentration on the order of 10 microM during a Ca^{2+} spark. *J. Gen. Physiol.* 120:15–27. doi:10.1085/jgp.20028571

ZhuGe, R., V. DeCrescenzo, V. Sorrentino, F.A. Lai, R.A. Tuft, L.M. Lifshitz, J.R. Lemos, C. Smith, K.E. Fogarty, and J.V. Walsh Jr. 2006. Syntillas release Ca^{2+} at a site different from the microdomain where exocytosis occurs in mouse chromaffin cells. *Biophys. J.* 90:2027–2037. doi:10.1529/biophysj.105.071654

ZhuGe, R., R. Bao, K.E. Fogarty, and L.M. Lifshitz. 2010. Ca2+ sparks act as potent regulators of excitation-contraction coupling in airway smooth muscle. *J. Biol. Chem.* 285:2203–2210. doi:10.1074/jbc.M109.067546

Zou, H., L.M. Lifshitz, R.A. Tuft, K.E. Fogarty, and J.J. Singer. 2002. Visualization of Ca2+ entry through single stretch-activated cation channels. *Proc. Natl. Acad. Sci. USA.* 99:6404–6409. doi:10.1073/pnas.092654999